Mechanism of strong enhancement of anomalous Nernst effect in Fe by Ga substitution

Hiroyasu Nakayama, Keisuke Masuda, Jian Wang, Asuka Miura, Ken-ichi Uchida, Masayuki Murata, and Yuya Sakuraba

Phys. Rev. Materials **3**, 114412 — Published 25 November 2019

DOI: 10.1103/PhysRevMaterials.3.114412

Mechanism of strong enhancement of anomalous Nernst effect in Fe by Ga substitution

Hiroyasu Nakayama[1,2,a)], Keisuke Masuda[2], Jian Wang[1,2], Asuka Miura[2], Ken-ichi Uchida[2,3,4,5], Masayuki Murata[6], and Yuya Sakuraba[2,7,b)]

[1]International Center for Young Scientists, National Institute for Materials Science, Tsukuba 305-0047, Japan
[2]Research Center for Magnetic and Spintronic Materials, National Institute for Materials Science, Tsukuba 305-0047, Japan
[3]Institute for Materials Research, Tohoku University, Sendai 980-8577, Japan
[4]Center for Spintronics Research Network, Tohoku University, Sendai 980-8577, Japan
[5]Department of Mechanical Engineering, The University of Tokyo, Tokyo 113-8656, Japan
[6]National Institute of Advanced Industrial Science and Technology, Tsukuba 305-8568, Japan
[7]PRESTO, Japan Science and Technology Agency, Saitama, 332-0012, Japan

a) Electronic mail: NAKAYAMA.Hiroyasu@nims.go.jp
b) Electronic mail: SAKURABA.Yuya@nims.go.jp

Abstract

We have investigated the anomalous Nernst effect (ANE) in $Fe_{1-x}Ga_x$ alloy films with different Ga atomic compositions ($x = 0 - 0.44$) deposited on MgO (001) single crystalline substrates. We found that the magnitude of the ANE increases with increasing x up to $x = 0.32$ even though the saturation magnetization decreases with increasing x. The magnitude of the ANE reaches to 2.4 μV/K in bcc $Fe_{0.68}Ga_{0.32}$ film, which is two orders of magnitude greater than that of pure Fe film. The magnetotransport measurements and the first-principles calculations revealed that the large ANE in bcc $Fe_{1-x}Ga_x$ is caused by the large transverse Peltier coefficient. The drastic enhancement of the transverse Peltier coefficient with increasing x can be attributed to small Fermi level tuning through the electron doping effect. Thus, we anticipate that our finding will provide a crucial piece of information to enhance the thermopower through the ANE.

Introduction

Thermoelectric power generation based on the thermoelectric phenomena has attracted a great deal of attention in terms of not only basic physics but also application for future environmental friendly power generation technologies, which aims to convert waste heat into electrical energy [1,2]. The most standard method to realize the thermoelectric power generation is utilizing the Seebeck effect [3,4]. The Seebeck effect converts temperature gradient to electric voltage in conductive materials thorough the diffusion of charge carrier [see Fig. 1(a)]. Another approach is to utilize the Nernst effect [5,6]. The Nernst effect is a phenomenon that generates electric voltage along the outer product of the temperature gradient and the applied magnetic field. Therefore, it is necessary to apply the external magnetic field to the thermoelectric materials in order to obtain the electric voltage induced by the Nernst effect. When we replace a thermoelectric material into a ferromagnet, however, it is not always necessary to apply the external magnetic field to obtain the magnetization direction dependent thermoelectric voltage. This phenomenon is known as the anomalous Nernst effect (ANE) [7–16]. The ANE is a phenomenon that generates electric voltage along the outer product of the temperature gradient and the magnetization in ferromagnet [see Fig. 1(b)]. The recently discovered longitudinal spin-Seebeck effect (SSE) induced inverse spin-Hall effect is known to exhibit similar symmetry as the ANE [17,18]. In the emerging field of spin-caloritronics, the ANE and the SSE play a leading role because these phenomena offer an approach to develop thermoelectric devices based on spin-heat coupling. In particular, the ANE in materials with a large anisotropy between electric and thermal conductivity and the SSE might go beyond the limitation of energy conversion efficiency by the Wiedemann-Franz law [2,14]. Recent works demonstrate that the thermoelectric voltage through the ANE and the SSE is dramatically enhanced by utilizing the simple lateral thermopile structures [12,19], which will pave the way towards the thermoelectric device such as a heat flow sensor with high flexibility, low thermal resistivity, and low cost [14]. However, it is still necessary to explore materials showing larger efficiency of thermoelectric conversion [14,20–22].

In order to develop an ANE device in this direction, it is an important issue to find materials consisting of abundant and nontoxic elements that exhibits large thermoelectric conversion efficiency. Therefore, the ANE in Fe-based compounds and alloys are worth to be investigated. Recently, the large ANE was reported in galfenol (Fe-Ga alloy) polycrystalline wire [23], where Fe-Ga alloys are known as magnetostrictive materials. Interestingly, it shows large thermopower of ANE (~ 3 μV/K) in simple binary alloy systems although the value in single crystalline bulk Fe is about -0.1 μV/K [24]. However, the previous work focused on the commercially available polycrystalline galfenol and its Ga composition is fixed at x = 0.15. Therefore, the underlying mechanism of the strong enhancement of the ANE from Fe to galfenol has not been clarified at all. In this study, we investigate the ANE in epitaxial Fe-Ga thin films with different compositions. We prepared $Fe_{1-x}Ga_x$ thin films on MgO (001) single crystalline substrates by co-sputtering technique. We found that the magnitude of the ANE in Fe-Ga alloys increases with increasing x up to x = 0.32 even when the crystal structure is preserved in the same simple bcc structure. The magnitude of the ANE reaches to 2.4 μV/K in $Fe_{0.68}Ga_{0.32}$ film, which is two orders of magnitude greater than that of Fe film [16]. The systematic thermoelectric and magnetotransport measurements including the Seebeck effect and the anomalous Hall effect measurements revealed that the large ANE in $Fe_{1-x}Ga_x$ is mainly attributed to the large transverse Peltier coefficient, which agrees with the prediction based on the first-principles calculations.

Methods

The samples were $Fe_{1-x}Ga_x$ thin films (Ga atomic composition x = 0 - 0.44) deposited on MgO (001) single crystalline substrates at room temperature by co-sputtering technique with Fe and $Fe_{0.50}Ga_{0.50}$ sputtering targets, where a base pressure was in the vicinity of 2×10^{-7} Pa. The thickness of the films was fixed at 40 nm, where the real thickness is determined by using the wavelength dispersive X-ray fluorescence analysis (WDXRF) and X-ray diffraction (XRD). In order to prevent films from oxidation, a 3-nm-thick MgO capping layer was deposited by rf magnetron sputtering. The composition of the $Fe_{1-x}Ga_x$ films was measured by WDXRF, where the Ga atomic composition was x = 0.44 when we fabricated $Fe_{1-x}Ga_x$ films by a $Fe_{0.50}Ga_{0.50}$ alloy target. The magnetic properties of the $Fe_{1-x}Ga_x$ films were measured with a vibrating sample magnetometer (VSM). The crystal structure was investigated by XRD with a Cu K_α X-ray source and a two-dimensional detector (PILATUS 100K/R, Rigaku Co.). Thin specimens for scanning transmission electron microscope (STEM) observations were prepared by the low-energy, low-angle Ar-ion milling using a precision ion polishing system (PIPS, GATAN Model-691). STEM observations were performed using a FEI Titan G2 80–200 STEM with a probe forming aberration corrector operated at

200 kV. A probe current of 100 pA was used for the STEM imaging. Element mapping was carried out by means of energy-dispersive X-ray spectroscopy (EDS) using an in-column symmetrically distributed four windowless silicon-drift X-ray detectors (SDD) that enable a high detection efficiency at atomic resolution. The Seebeck effect was measured by using the Seebeck Coefficient/Electric Resistance Measurement System (ZEM-3, ADVANCE RIKO, Inc.). The substrates were cleaved into a piece with a lateral dimension of $\sim 7.6 \times 10.0$ mm^2. The films were patterned into a Hall bar structure with a width of 3.0 mm and a length of 7.0 mm by using photolithography and Ar ion milling. The anomalous Hall effect (AHE) measurements were conducted at room temperature and 10 K with applying the perpendicular magnetic field by using a Physical Property Measurement System (PPMS, Quantum Design Co., Ltd.). The ANE was also measured at room temperature with applying perpendicular magnetic field in PPMS. The Seebeck effect was also measured simultaneously to calibrate the applied temperature gradient. The relationship between the applied temperature gradient and the Seebeck voltage in FeGa film was confirmed at outside of PPMS in advance by utilizing an infrared thermal camera, where the sample surface is coated by black ink. Then, the applied temperature gradient was calibrated through the observed Seebeck voltage in PPMS. Here, the thermal conductance of the MgO substrate is much greater than that of $Fe_{1-x}Ga_x$ thin films, which results in the fact that the thermal conductance of $Fe_{1-x}Ga_x$ thin films does not influence the temperature gradient in the films [25]. The electric resistivity was measured by a dc four-probe method with a constant dc current of 300 μA. All the measurements, except for the AHE measurements at 10 K, were performed at room temperature.

Experimental results & Discussions

To characterize the magnetic and structural properties of the $Fe_{1-x}Ga_x$ thin films, we conducted the VSM, the XRD, and the TEM measurements. Figure 2(a) shows the out-of-plane XRD pattern for $Fe_{1-x}Ga_x$ thin films. In order to clearly show the diffraction peak from $Fe_{1-x}Ga_x$ thin films, we subtracted the XRD pattern of a MgO (001) substrate without $Fe_{1-x}Ga_x$ thin films. As shown in Fig. 2(a), only (002) peak from the simple bcc $Fe_{1-x}Ga_x$ are observed for all of the samples except for $x = 0.44$. In a $Fe_{0.54}Ga_{0.44}$ film, the super lattice (001) peak of B2-FeGa is also observed in the vicinity of $2\theta = 31^{\circ}$. These results clearly show that all the $Fe_{1-x}Ga_x$ thin films are epitaxially grown. Figure 2(b) shows the cross-sectional high-angle annular dark-field scanning transmission electron microscopy (HAADF-STEM) image and corresponding energy-dispersive X-ray spectroscopy (EDS) elemental maps of $Fe_{0.81}Ga_{0.19}$ film. In Fig. 2(b), one can find the continuous layer with flat surface and uniform Ga distribution in the $Fe_{0.81}Ga_{0.19}$ film, whereas the slight segregation of Ga exists at the surface and interface. The slight contrast of HAADF-STEM image in Fig. 2(b) can be due to the surface damage caused by Ar ion milling using PIPS. Figure 2(c) shows the x dependence of lattice constant determined from position of (002) peak in Fig. 2(a). In our $Fe_{1-x}Ga_x$ (x = 0 - 0.44) films, the (002) peak gradually shifts toward lower angle with increasing Ga, thus lattice constant almost monotonically increases with increasing x. These results indicate that Ga replaces Fe without structural transformation despite the fact that the solubility of Ga to Fe is less than 15 at.% at room temperature in the equilibrium binary phase diagram [26], suggesting that our sputtered $Fe_{1-x}Ga_x$ films have the non-equilibrum bcc structure in which Ga randomly occupied Fe site up to 32 at.%. Figure 2(d) shows the Ga composition x dependence of the saturation magnetization M_s for $Fe_{1-x}Ga_x$ thin films, where M_s is determined by using VSM with in-plane magnetic field along the [001] orientation for $Fe_{1-x}Ga_x$ thin films [also see the inset of Fig. 2(d)]. The M_s decreases with increasing x, which can be due to the replacement of Fe atoms with Ga atoms. The decreasing tendency of M_s with increasing x is consistent with the theoretically calculated M_s plotted as open circles in Fig. 2(d). Here, the theoretically calculated M_s is obtained by the first-principles calculations using the Akai-KKR code [27], the details of which will be explained later.

To investigate the mechanism of the ANE in $Fe_{1-x}Ga_x$ thin films, we conducted the AHE measurements. Figure 3 shows the anomalous Hall resistivity ρ_{yx} plotted as a function of the magnetic field $\mu_0 H$ along the z axis in the $Fe_{1-x}Ga_x$ thin films. The inset shows a schematic illustration of an experimental configuration of the AHE measurements. As one can clearly see in Fig. 3, the magnitude of the ρ_{yx} increases with increasing x. The magnetization reversal field of $Fe_{1-x}Ga_x$ thin films tends to decrease with increasing x, which corresponds to the decreasing of the demagnetization field due to the reduction of the saturation magnetization M_s in $Fe_{1-x}Ga_x$ thin films with increasing x. As shown in Figs. 4(a)-4(c), the ρ_{yx} and the ρ_{xx} increase with increasing x, whereas the magnitude of $|\theta_{AHE}|$ exhibits a maximum value in the vicinity of $x = 0.16$. As shown in Fig. 4(d), the $|\sigma_{xy}|$ tends to decrease with increasing x in both 10 K and 300 K. The inset of 4(d) shows the $|\sigma_{xy}|$ dependence of σ_{xx}. The solid line for lower (larger) σ_{xx} is the fit according to the scaling relationship $|\sigma_{xy}| \propto \sigma_{xx}^{n}$ with $n = 1.6$ ($n = 0$), which corresponds to the scaling behavior in a dirty region (intrinsic moderately dirty region).

In order to investigate the origin of large AHE in Fe-Ga thin films, we calculated the density of states (DOS) of Fe-Ga with bcc structure by using the Akai-KKR code [27] based on the density-functional theory and the Korringa-Kohn-Rostoker method [28,29]. The generalized gradient approximation [30] was adopted for the exchange-correlation energy and the chemical disorder between Fe and Ga atoms was treated by the approximation. We set the lattice constants of Fe, $\mathrm{Fe_{0.9}Ga_{0.1}}$, and $\mathrm{Fe_{0.8}Ga_{0.2}}$ to 2.853, and 2.861 Å, respectively, which were determined following the Vegard's law by the linear fit to the data ($x = 0$ - 0.32) of Fig. 2(c) with the fixed value of ($x = 0$, $a = 2.846$ Å). In our calculations, 5832 (= 18 × 18 × 18) k points were for the Brillouin-zone integration and the imaginary part of the energy was as 0.001 Ry. Figure 5(a) shows the DOSs of Fe, $\mathrm{Fe_{0.9}Ga_{0.1}}$, and $\mathrm{Fe_{0.8}Ga_{0.2}}$, where indicates the Fermi level. With increasing the Ga content, the DOS moves to energies keeping the overall energy dependence; namely, the effect of the Ga doping into bcc Fe can be considered as a rigid-band shift of the band structure of bcc Fe. Figure 5(b) shows the projected density of state (PDOS) of Fe and $\mathrm{Fe_{0.8}Ga_{0.2}}$, from which we see that the energy shift of the total DOS mainly from that of the Fe PDOS. Such an energy shift in the Fe PDOS can be as an electron-doping effect from Ga *s* and *p* orbitals to Fe *d* orbitals. Actually, as shown in Figs. 5(c) and 5(d), Ga *s* and *p* orbitals in $\mathrm{Fe_{0.8}Ga_{0.2}}$ have finite PDOSs around ε_F, indicating that electrons in these orbitals can contribute to the electron doping into Fe *d* orbitals. Therefore, it is reasonable to discuss a tendency of and ANE against Ga concentration x based on the theoretical calculation of dependence of those in pure Fe. Previously Weischenberg *et al*. performed the *ab-initio* calculation of the contribution of intrinsic mechanism on AHE in Fe and reported the energy dependence of $\sigma_{xy}^{\mathrm{int}}$ in Fe [31]. Thus, here we argue the tendency of AHE against Ga concentration in $\mathrm{Fe_{1\text{-}x}Ga_x}$ films on the basis of their calculation for pure Fe. In the theoretical calculation, $\sigma_{xy}^{\mathrm{int}}$ at ε_F in Fe is about S/cm and tends to decrease with increasing ε to about 400 S/cm at $\varepsilon_\mathrm{F} + 0.5$ Experimentally observed $|\sigma_{xy}|$ shows almost monotonic reduction with x except the drastic increase at $x = 0.03$ [see Fig. 4(d)], which roughly agree with the dependence of the theoretical $\sigma_{xy}^{\mathrm{int}}$. The smaller magnitude of the experimentally determined $|\sigma_{xy}|$ in our epitaxial $\mathrm{Fe_{1\text{-}x}Ga_x}$ films with large x than that of the theoretically calculated $\sigma_{xy}^{\mathrm{int}}$ can be explained by the existence of the damping the intrinsic mechanism of the AHE due to the electron scattering at the surface and substrate interface [32]. Since we evaluated σ_{xy} using $\sigma_{xy} = \rho_{yx}/\rho_{xx}^2$ with the experimentally observed ρ_{yx} and ρ_{xx} shown in Figs. 4(a) and 4(b), abovementioned scattering that increases residual resistance causes the reduction of σ_{xy} compared with the theoretically calculated $\sigma_{xy}^{\mathrm{int}}$, where the Berry curvature of intrinsic electronic structure determines the magnitude of $\sigma_{xy}^{\mathrm{int}}$. Large contribution of the residual resistance in higher x region can be also confirmed by small RRR shown in Fig. 4(b). Although a mechanism of the enhancement of σ_{xy} at $x = 0.03$ shown in Fig. 4(d) has not been clarified, the contribution of extrinsic anomalous Hall effect, skew scattering, can be the possible reason. The σ_{xy} at 10 K and 300 K in $\mathrm{Fe}_{1-x}\mathrm{Ga}_x$ film with $x = 0.03$ shown in Fig. 4(d) exhibit much larger difference than those of $\mathrm{Fe}_{1-x}\mathrm{Ga}_x$ films with greater x, which can be an evidence of the existence of skew scattering contribution because the skew scattering term of AHE $\sigma_{xy}^{\mathrm{skew}}$ is proportional to σ_{xx}, i.e., $\sigma_{xy}^{\mathrm{skew}} \propto \sigma_{xx}$ whereas $\sigma_{xy}^{\mathrm{int}}$ is independent of σ_{xx}, i.e., $\sigma_{xy}^{\mathrm{int}} \propto \sigma_{xx}^0$ [33,34].

Figure 6 shows the observed ANE voltage normalized by the width and applied temperature gradient $(V_{\mathrm{ANE}}/w)\nabla T$ plotted as a function of the external magnetic field $\mu_0 H$ along the z axis in $\mathrm{Fe}_{1-x}\mathrm{Ga}_x$ thin films. The thermopower of the ANE S_{ANE} corresponds to the linearly extrapolated value of $(V_{\mathrm{ANE}}/w)\nabla T$ to zero magnetic field from the saturated value at high magnetic field. The inset shows a schematic of the experimental configuration of the ANE measurements. In Fig. 6, one can clearly find that the S_{ANE} tends to increase by Ga substitution in Fe with increasing x up to $x = 0.32$. Figures 7(a)-7(b) show the x dependence of (a) the Seebeck coefficient S_{SE}, (b) the S_{ANE}. Previous studies analyzed the ANE signal by separating S_{ANE} into two components based on the following linear response equation [8,10],

$$S_{\mathrm{ANE}} = \rho_{xx}\alpha_{xy} + \rho_{xy}\alpha_{xx} \qquad (1)$$

The second term $\rho_{xy}\alpha_{xx}$ (defined as S_{II} here) can be converted to - $S_{\mathrm{SE}} \times \tan\theta_{\mathrm{AHE}}$, thus this term can be regarded as the transverse thermopower generation from the AHE of longitudinal carrier flow induced by the Seebeck effect. On the other hand, the first term $\rho_{xx}\alpha_{xy}$ (defined as S_{I} here) can be considered as an intrinsic term of the ANE because the transverse Peltier coefficient α_{xy} gives a direct conversion of applied temperature gradient to transverse current as expressed with $j_y = \alpha_{xy}\nabla T_x$. Therefore, we also evaluate S_{I} and S_{II} contributions of the observed ANE in our $\mathrm{Fe}_{1-x}\mathrm{Ga}_x$ thin films as shown in Fig. 7(c). In Fig. 7(a), the $|S_{\mathrm{SE}}|$ exhibits local maximal value in the vicinity of $x = 0.2$. The S_{SE} also exhibits sign reversal in the vicinity of x = 0.02, which presumably due to the Fermi energy shift because the Seebeck coefficient is proportional to $dN(\varepsilon)/d\varepsilon$ [35]. As one can see in Fig. 7(b), the magnitude of the ANE reaches to 2.4 μV/K in $Fe_{0.68}Ga_{0.32}$ film, which is two orders of magnitude greater than that of Fe film [16]. The anomalous Nernst coefficient Q in $Fe_{0.68}Ga_{0.32}$ film is 2.2 $\mu VT^{-1}K^{-1}$, which is same order of magnitude as that of polycrystalline $Fe_{0.85}Ga_{0.15}$ wire (Fe-Al thin film) reported in the previous works [16,23]. The inset of Fig. 7(b) shows the M_s dependence of the S_{ANE}, clearly indicating that the S_{ANE} decreases with increasing the M_s when $M_s > 1.1$ T, which is completely different from the scaling behavior obtained for various ferromagnetic materials. In Fig. 7(b), the S_{ANE} increases with increasing x up to x = 0.32 even though the $|\theta_{AHE}|$ in $Fe_{1-x}Ga_x$ thin films exhibits the largest value in the vicinity of x = 0.16 [also see Fig. 4(c)]. This difference of Ga concentration x dependence between the AHE and the ANE can be understood by considering the possible contribution of the ANE: S_I and S_{II}. As shown in Fig. 7(c), the dominant contribution of the ANE switches in the vicinity of x = 0.2 in $Fe_{1-x}Ga_x$ films; S_I and S_{II} comparably appears in the films with $x < 0.2$, but the contribution of S_I is dominant with $x > 0.2$. These results indicate that the longitudinal resistivity ρ_{xx} and the transverse Peltier coefficient α_{xy} are critical parameters for large S_{ANE} rather than the Seebeck coefficient and the anomalous Hall angle in $Fe_{1-x}Ga_x$ thin films with $x > 0.2$. Therefore, the origin of the large ANE in $Fe_{0.68}Ga_{0.32}$ film is quite different from the case in ferromagnetic materials such as $Co_2MnAl_{1-x}Si_x$ [22] and Co_2MnGa [21] in which both S_I and S_{II} contribute comparably. Figure 7(d) shows the x dependence of experimentally determined transverse Peltier coefficient α_{xy}. As shown in Fig. 7(d), the α_{xy} exhibits oscillation behavior with x.

According to the generalized Mott formula [31,36–38], the relation between the σ_{xy} and the α_{xy} at the fixed temperature T is described as

$$\alpha_{xy} = -\frac{1}{eT}\int d\varepsilon \frac{\partial f}{\partial \mu}(\varepsilon - \mu)\sigma_{xy} \qquad (2),$$

where e, f, and μ are the electronic charge ($e = -|e|$), the Fermi distribution function, and the chemical potential. In Eq. (2), the integrand becomes finite in the range of ~ 0.1 eV at 300 K due to the existence of $\partial f/\partial \mu$. Here, $\partial f/\partial \mu$ and $(\varepsilon - \mu)$ are even and odd functions of ε at around μ, respectively. If σ_{xy} is odd function, the integrand in Eq. (2) becomes even function. Thus, the magnitude and the sign of the odd function in σ_{xy} at around ε_F determines the magnitude and the sign of the α_{xy}. Here we compare the experimental α_{xy} with theoretical value predicted from the $\sigma_{xy}^{\mathrm{int}}(\varepsilon)$ in pure Fe [31]. In Fe, the $\sigma_{xy}^{\mathrm{int}}(\varepsilon)$ was predicted to behave like the even function of the ε at around ε_F [31]. Therefore, even though the $\sigma_{xy}^{\mathrm{int}}$ at ε_F is large in Fe, the magnitude of the theoretical α_{xy} in Fe becomes very small ~ +0.15 A/(m·K), which shows good agreement with experimentally evaluated α_{xy}, +0.13 A/(m·K). By looking carefully at the theoretically calculated $\sigma_{xy}^{\mathrm{int}}$ in Fe [31], one can find that $\sigma_{xy}^{\mathrm{int}}(\varepsilon)$ exhibits almost continuous reduction against ε from 0 to +0.5 eV with two shoulders at the vicinity of $\varepsilon - \varepsilon_F = \sim 0.08$ and ~ 0.32 eV, indicating that $\alpha_{xy}(\varepsilon)$ is expected to have two peaks at around these two energies corresponding to the shoulders in pure Fe due to enhancement of $|\partial\sigma_{xy}^{\mathrm{int}}/\partial\varepsilon|$. It is interesting to see that experimental α_{xy} in $Fe_{1-x}Ga_x$ films also shows two peaks at the vicinity of $x = 0.1$ and 0.3 in Fig. 7(d). The theoretical α_{xy} given in Ref. 31 at $\varepsilon - \varepsilon_F = \sim 0.08$ eV is 0.96 A/(m·K) at 300 K, which also agrees well with experimental α_{xy} ~ 1.1 A/(m·K) in $Fe_{0.90}Ga_{0.10}$ film. Although it is difficult to strictly evaluate the actual ε_F shift of Fe by Ga substitution from the calculated DOS in Fig. 5, the rough evaluation gives the value of about 0.1 - 0.2 eV shift in $Fe_{0.9}Ga_{0.1}$, which almost agrees with the theoretically predicted first peak position ~ 0.08 eV for pure Fe. The deviation of the peak position of α_{xy} between experimental x dependence in $Fe_{1-x}Ga_x$ films and the theoretical predicted energy in pure Fe is more or less attributed to the slight segregation of Ga at the surface and interface as shown in Fig. 2(b). Therefore, we concluded that the enhancement of the ANE in Fe by Ga substitution originates from the enhancement of intrinsic α_{xy} because of the Fermi level shifting of Fe. It should be mentioned here that Weischenberg *et al*. has also calculated the anomalous Hall conductivity arising from the extrinsic mechanism, i.e. side jump mechanism, $\sigma_{xy}^{\mathrm{side}}$ in Ref. 31. In Fe, $\sigma_{xy}^{\mathrm{side}}$ was predicted to be much smaller than intrinsic $\sigma_{xy}^{\mathrm{int}}$ at ε_F, about 110 S/cm. In contrast to $\sigma_{xy}^{\mathrm{int}}$, however, $\sigma_{xy}^{\mathrm{side}}$ was predicted to increase with ε and takes a peak of about 300 S/cm at the vicinity of 0.25 eV although the situation $\sigma_{xy}^{\mathrm{int}} > \sigma_{xy}^{\mathrm{side}}$ maintains in the range of $0 \leq \varepsilon < 0.5$ eV. It seems that our experimental result of AHE and ANE in $Fe_{1-x}Ga_x$ films can be explained by the energy dependence of only $\sigma_{xy}^{\mathrm{int}}$, suggesting that the contribution of $\sigma_{xy}^{\mathrm{side}}$ is not remarkable in our $Fe_{1-x}Ga_x$ thin films. However, further investigation is required to consider the contribution of side jump mechanism on ANE. Here, it is also worth mentioning that one might have an interest in the relationship between the ANE and the magnetostriction of Fe-Ga. Although the magnetostriction in our $Fe_{1-x}Ga_x$ thin films has not been measured in this study, we could not find clear relationship in the Ga composition dependence of the magnitude between the observed ANE and the reported magnetostriction in Fe-Ga [39].

Conclusion

The anomalous Nernst effect (ANE) has been investigated in $Fe_{1-x}Ga_x$ alloy with different Ga atomic compositions in the range of $x = 0$ - 0.44. We fabricated $Fe_{1-x}Ga_x$ thin films on MgO (001) single crystalline substrates by co-sputtering technique. We found that the magnitude of the ANE in $Fe_{1-x}Ga_x$ alloys increases with increasing x up to $x = 0.32$, where the simple bcc crystal structure is preserved in $Fe_{0.68}Ga_{0.32}$ film. The magnitude of the ANE in $Fe_{0.68}Ga_{0.32}$ film reaches to 2.4 μV/K, which is two orders of magnitude greater than that of Fe film. The systematic magnetotransport measurements and the first-principles calculations revealed that the large ANE in $Fe_{1-x}Ga_x$ is due to the large transverse Peltier coefficient α_{xy}. The maximum value of the theoretically calculated α_{xy} shows good agreement with the experimentally determined values in $Fe_{1-x}Ga_x$. The large enhancement of the ANE in Fe by replacing Fe atoms into Ga atoms can be mainly attributed to the shift of the Fermi energy, which can be understood as the electron doping effect. This kind of approach based on the Fermi energy engineering can be applicable to other magnetic materials. Therefore, our finding will provide crucial information to enhance the thermoelectric power through the ANE in various magnetic (ferro-, ferri- and anti-ferromagnetic) materials and pave the way to practical applications using ANE.

Acknowledgments

We would like to thank A. Yamamoto, K. Nawa, S. Isogami, and H. Fujita for valuable discussions and N. Kojima, B. Masaoka, J. W. Jung, and W. Zhou for technical supports. This work was supported in part by JSPS KAKENHI Grants No. 26709045, No. 19H02585, No. 19K15297, No. 18J02115, No. 17H04808, PRESTO “Scientific Innovation for Energy Harvesting Technology”(JPMJPR12C1) and CREST “Creation of Innovative Core technologies for nano-enabled Thermal Managemnent”(JPMJCR1711) , and the NEDO. A. M. is supported by JSPS thorough Research Fellowship for Young Scientists (JP18J02115). H.N. and J.W would like to acknowledge the ICYS Research Fellowship, NIMS, Japan.

References

[1] G. E. W. Bauer, E. Saitoh, and B. J. van Wees, Nat. Mater. **11**, 391 (2012).

[2] K. Uchida, H. Adachi, T. Kikkawa, A. Kirihara, M. Ishida, S. Yorozu, S. Maekawa, and E. Saitoh, Proc. IEEE **104**, 1946 (2016).

[3] G. D. Mahan, Solid State Phys. **51**, 81 (1998).

[4] G. J. Snyder and E. S. Toberer, Nat. Mater. **7**, 105 (2008).

[5] W. Nernst, Ann. Phys. **267**, 760 (1887).

[6] K. Behnia, M. A. Méasson, and Y. Kopelevich, Phys. Rev. Lett. **98**, 076603 (2007).

[7] R. Suryanarayanan, V. Gasumyants, and N. Ageev, Phys. Rev. B **59**, R9019(R) (1999).

[8] W. L. Lee, S. Watauchi, V. L. Miller, R. J. Cava, and N. P. Ong, Phys. Rev. Lett. **93**, 226601 (2004).

[9] T. Miyasato, N. Abe, T. Fujii, A. Asamitsu, S. Onoda, Y. Onose, N. Nagaosa, and Y. Tokura, Phys. Rev. Lett. **99**, 086602 (2007).

[10] Y. Pu, D. Chiba, F. Matsukura, H. Ohno, and J. Shi, Phys. Rev. Lett. **101**, 117208 (2008).

[11] M. Mizuguchi, S. Ohata, K. Uchida, E. Saitoh, and K. Takanashi, Appl. Phys. Express **5**, 093002 (2012).

[12] Y. Sakuraba, K. Hasegawa, M. Mizuguchi, T. Kubota, S. Mizukami, T. Miyazaki, and K. Takanashi, Appl. Phys. Express **6**, 033003 (2013).

[13] K. Hasegawa, M. Mizuguchi, Y. Sakuraba, T. Kamada, T. Kojima, T. Kubota, S. Mizukami, T. Miyazaki, and K. Takanashi, Appl. Phys. Lett. **106**, 252405 (2015).

[14] Y. Sakuraba, Scr. Mater. **111**, 29 (2016).

[15] T. C. Chuang, P. L. Su, P. H. Wu, and S. Y. Huang, Phys. Rev. B **96**, 174406 (2017).

[16] S. Isogami, K. Takanashi, and M. Mizuguchi, Appl. Phys. Express **10**, 073005 (2017).

[17] K. Uchida, H. Adachi, T. Ota, H. Nakayama, S. Maekawa, and E. Saitoh, Appl. Phys. Lett. **97**, 172505 (2010).

[18] T. Kikkawa, K. Uchida, Y. Shiomi, Z. Qiu, D. Hou, D. Tian, H. Nakayama, X. F. Jin, and E. Saitoh, Phys. Rev. Lett. **110**, 067207 (2013).

[19] K. Uchida, T. Nonaka, T. Yoshino, T. Kikkawa, D. Kikuchi, and E. Saitoh, Appl. Phys. Express **5**, 093001 (2012).

[20] M. Ikhlas, T. Tomita, T. Koretsune, M. T. Suzuki, D. Nishio-Hamane, R. Arita, Y. Otani, and S. Nakatsuji, Nat. Phys. **13**, 1085 (2017).

[21] A. Sakai, Y. P. Mizuta, A. A. Nugroho, R. Sihombing, T. Koretsune, M. T. Suzuki, N. Takemori, R. Ishii, D. Nishio-Hamane, R. Arita, P. Goswami, and S. Nakatsuji, Nat. Phys. **14**, 1119 (2018).

[22] Y. Sakuraba, K. Hyodo, A. Sakuma, and S. Mitani, ArXiv :1807.02209 (2018).

[23] Z. Yang, E. A. Codecido, J. Marquez, Y. Zheng, J. P. Heremans, and R. C. Myers, AIP Adv. **7**, 095017 (2017).

[24] S. J. Watzman, R. A. Duine, Y. Tserkovnyak, S. R. Boona, H. Jin, A. Prakash, Y. Zheng, and J. P. Heremans, Phys. Rev. B **94**, 144407 (2016).

[25] C. Fang, C. H. Wan, Z. H. Yuan, L. Huang, X. Zhang, H. Wu, Q. T. Zhang, and X. F. Han, Phys. Rev. B **93**, 054420 (2016).

[26] H. Okamoto, J. Phase Equilibria Diffus. **25**, 100 (2004).

[27] H. Akai, http://kkr.issp.u (2002).

[28] J. Korringa, Physica **13**, 392 (1947).

[29] W. Kohn and N. Rostoker, Phys. Rev. **94**, 1111 (1954).

[30] J. P. Perdew, K. Burke, and M. Ernzerhof, Phys. Rev. Lett. **77**, 3865 (1996).

[31] J. Weischenberg, F. Freimuth, S. Blügel, and Y. Mokrousov, Phys. Rev. B **87**, 060406(R) (2013).

[32] S. Sangiao, L. Morellon, G. Simon, J. M. De Teresa, J. A. Pardo, J. Arbiol, and M. R. Ibarra, Phys. Rev. B **79**, 014431 (2009).

[33] J. Smit, Physica **21**, 877 (1955).

[34] S. Onoda, N. Sugimoto, and N. Nagaosa, Phys. Rev. B **77**, 165103 (2008).

[35] F. J. Blatt, P. A. Schroeder, C. L. Foiles, and D. Greig, *Thermoelectric Power of Metals, Plenum Press, New York* (1976).

[36] L. Smrčka and P. Streda, J. Phys. C **10**, 2153 (1977).

[37] M. Jonson and G. D. Mahan, Phys. Rev. B **21**, 4223 (1980).

[38] M. J. Kearney and P. N. Butcher, J. Phys. C **21**, L265 (1988).

[39] J. B. Restorff, M. Wun-Fogle, K. B. Hathaway, A. E. Clark, T. A. Lograsso, and G. Petculescu, J. Appl. Phys. **111**, 023905 (2012).

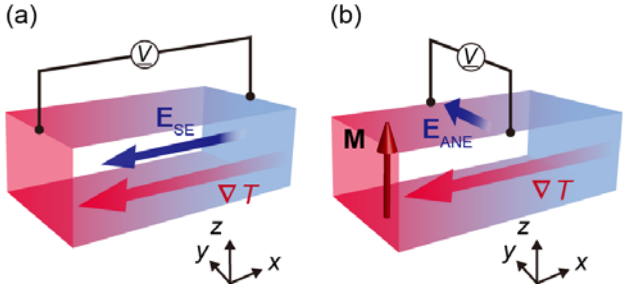

FIG. 1. Schematic of experimental configuration for (a) the Seebeck effect and (b) the anomalous Nernst effect (ANE) measurements. $\mathbf{E}_{\mathrm{SE}}$, $\mathbf{E}_{\mathrm{ANE}}$, $\mathbf{M}$, and ∇T denote the electric field induced by the Seebeck effect and the ANE, the magnetization vector of the ferromagnets, and the applied temperature gradient, respectively.

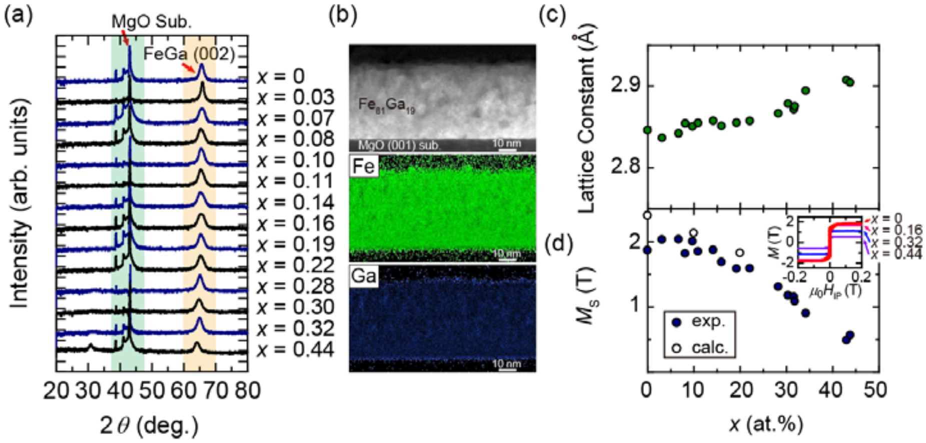

FIG. 2. (a) Out-of-plane XRD pattern for $Fe_{1-x}Ga_x$ thin films. In order to clearly show XRD pattern for $Fe_{1-x}Ga_x$ thin films, we subtracted the XRD pattern of MgO (001) a substrate without $Fe_{1-x}Ga_x$ thin films. Because the subtraction was conducted for two-dimensional diffraction images of the substrate with and without films, the slight difference of the tilting of the substrate between two measurements causes a variation of remaining intensity from the MgO substrate in the vicinity of $2\theta = 42^{\circ}$. (b) Cross-sectional HAADF-STEM images and corresponding EDS maps for $Fe_{0.81}Ga_{0.19}$ film. (c) Ga composition x dependence of lattice constant determined from position of (002) peak. (d) x dependence of saturation magnetization M_s for $Fe_{1-x}Ga_x$ thin films, where the open circles are the theoretically calculated values for Fe, $Fe_{0.9}Ga_{0.1}$, and $Fe_{0.8}Ga_{0.2}$. The inset shows the in-plane magnetic field along [001] orientation $\mu_0 H_{\mathrm{IP}}$ dependence of the magnetization M for $Fe_{1-x}Ga_x$ thin films.

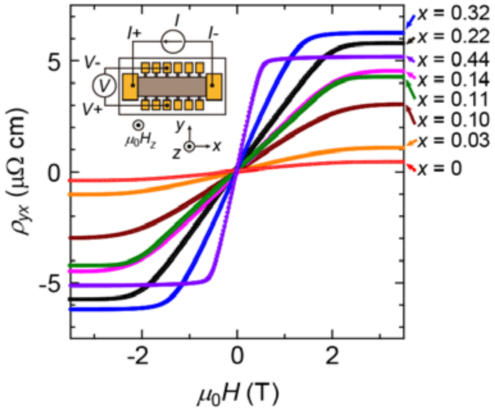

FIG. 3. The anomalous Hall resistivity plotted as a function of the magnetic field $\mu_0 H$ along the z axis in the $Fe_{1-x}Ga_x$ thin films. The inset shows a schematic of the experimental configuration of the anomalous Hall effect (AHE) measurements.

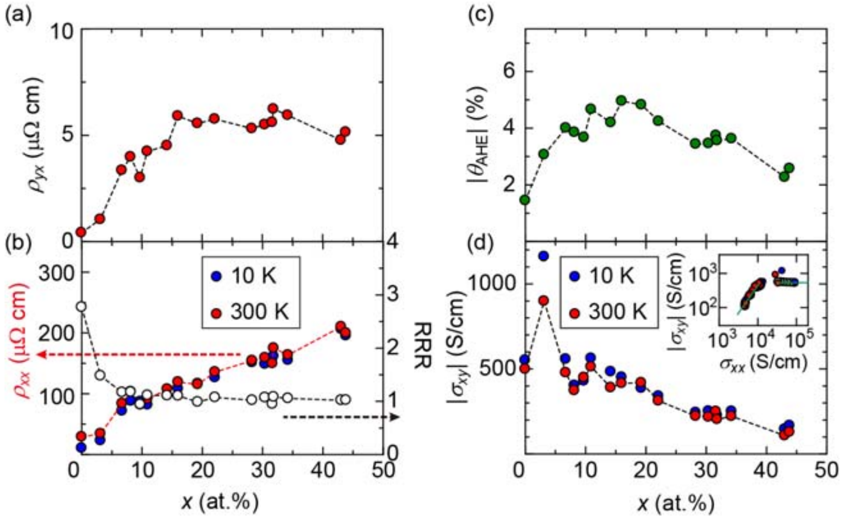

FIG. 4. The Ga composition x dependence of (a) the anomalous Hall resistivity ρ_{yx}, (b) the longitudinal resistivity ρ_{xx} (red and blue plots) and the residual resistivity ratio RRR (open circles) defined as $\rho_{xx}(300\ \text{K})/\rho_{xx}(10\ \text{K})$, (c) the anomalous Hall angle $|\theta_{\text{AHE}}|$ $(= |\rho_{yx}/\rho_{xx}|)$, and (d) the anomalous Hall conductivity $|\sigma_{xy}|$ (red and blue plots) in $Fe_{1-x}Ga_x$ thin films, where the blue (red) plot in Figs. 4(b) and 4(d) are measured at 10 K (300 K). The inset shows the $|\sigma_{xy}|$ dependence of the electrical conductivity σ_{xx}, where the solid line for lower (larger) σ_{xx} corresponds to the fit according to the scaling relationship $|\sigma_{xy}| \propto \sigma_{xx}^{n}$ with $n = 1.6$ ($n = 0$).

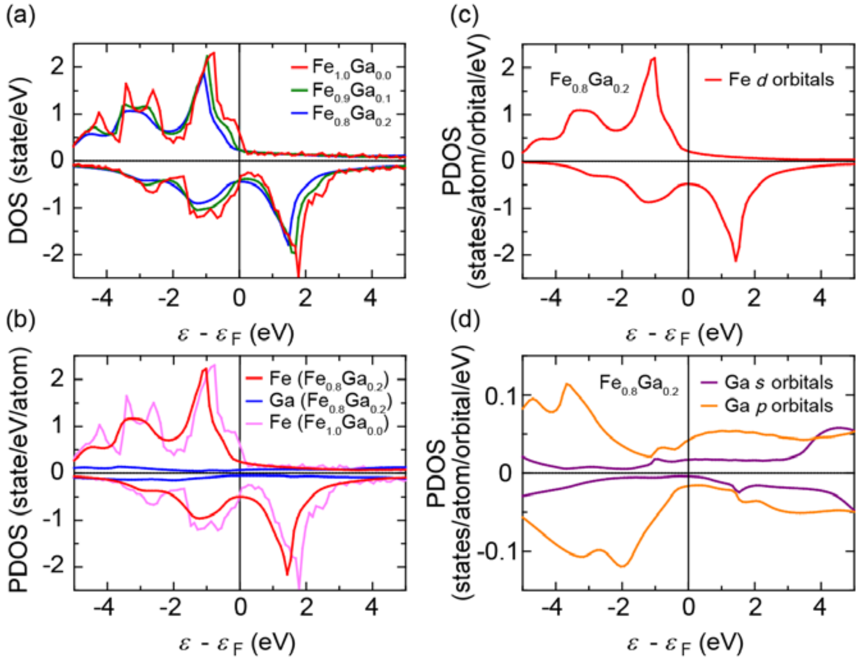

FIG. 5. (a) The DOSs of Fe, $Fe_{0.9}Ga_{0.1}$, and $Fe_{0.8}Ga_{0.2}$, where ε_F is the Fermi level. (b) The PDOSs of Fe and $Fe_{0.8}Ga_{0.2}$. (c) and (d) The orbital-resolved PDOSs in Fe *d* and Ga *s* and *p* orbitals of $Fe_{0.8}Ga_{0.2}$.

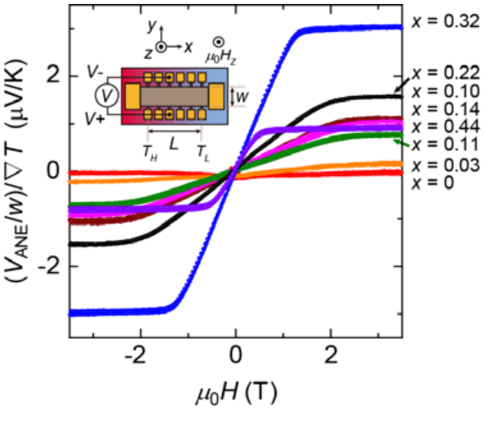

FIG. 6. The $\mu_0 H$ dependence of the observed ANE voltage V_{ANE} along the *y* axis normalized by the width of the Hall bar structure *w* and the applied temperature gradient ∇T along the *x* axis for $Fe_{1-x}Ga_x$ thin films. The inset shows a schematic of the experimental configuration of the ANE measurements.

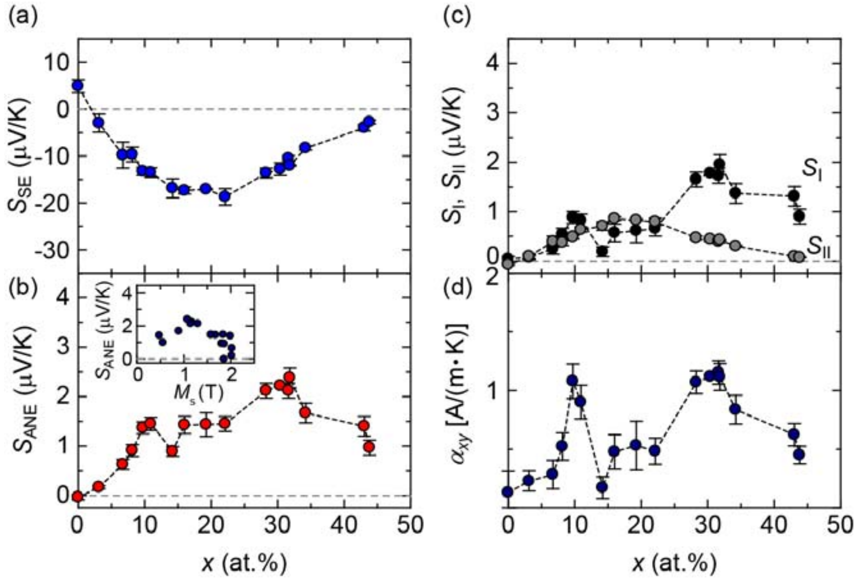

FIG. 7. The Ga composition x dependence of (a) the Seebeck coefficient S_{SE}, (b) the magnitude of the ANE S_{ANE} in $Fe_{1-x}Ga_x$ thin films. The inset shows M_s dependence of the S_{ANE}. x dependence of (c) S_I and S_{II}, where $S_I = \alpha_{xy}\rho_{xx}$ and $S_{II} = -S_{SE} \times \tan\theta_{AHE}$ in $Fe_{1-x}Ga_x$ thin films, and (d) the transverse Peltier coefficient α_{xy} in $Fe_{1-x}Ga_x$ thin films.